Tortuosity of Bubble Rise Path in a Liquid-Solid Fluidized Bed: Effect of Particle Shape

Katsumi Tsuchiya and Akihiko Furumoto
Dept. of Chemical Science and Technology, University of Tokushima, Tokushima 770, Japan

Effects of particle properties on the rise of single bubbles in a liquid–solid fluidized bed are studied by focusing on the particle-shape effect at various bed voidages near incipient fluidization of glass beads and sand particles. Experiments, covering the bubble-size range 6–37 mm and solids holdups as high as 0.94 times that in the packed state, are conducted in a 2-D column to directly observe the possible relationship between the rate and tortuous path of bubble rise. The shape effect, being significant when the close-range (surface-to-surface) interactions between the particles are predominant, is appreciable for the relative solids holdups exceeding 0.9. Marked reduction in the bubble rise velocity is observed as the bubble size is decreased below 8 and 12 mm for the spherical glass and irregular sand particles, respectively. This anomalous reduction stems partly from the tortuousness in the rise path and partly from the "hesitation" in the net vertical movement. The former, in particular, is quantified in terms of the tortuosity of the 2-D rise path. The results support the peculiar trend in the rise velocity observed, especially for the sand particles.

Introduction

In the hydrodynamics and mass- and heat-transfer characteristics of gas–liquid(–solid) systems such as bubble columns and three-phase fluidized beds, the bubble rise velocity plays a variety of crucial roles directly or indirectly. For instance, it is a measure of the reciprocal of the residence time of the gas phase, thus directly influencing the determination of the gas holdup; when set relative to the linear velocity of the surrounding flow, usually flowing liquid, it controls the dynamics (such as instability) of the flow behind bubbles or the bubble wake, which in turn contribute to the mixing behavior of the liquid and solid phases (Fan and Tsuchiya, 1990); furthermore, for single/isolated rising bubbles it is closely related to the gas–liquid mass-transfer rate (Higbie, 1935).

While the rise of a single gas bubble in liquids has been investigated extensively (Clift et al., 1978), pertinent studies in liquid–solid fluidized beds are not as extensive but are being accumulated: for three-dimensional systems, Massimilla et al. (1961), Darton and Harrison (1974), Verbitskii and Vakhrushev (1975), Jang (1989), Jean and Fan (1990), and Bly and Worden (1992); for two-dimensional systems, Henriksen and Ostergaard (1974), El-Temtamy and Epstein (1980), and Tsuchiya et al. (1990). The most crucial (and difficult) point to be addressed is how to deal with the liquid–solid medium with respect to the rising bubble as an isolated entity—*homogeneous* or *heterogeneous*. The homogeneous concept (Darton and Harrison, 1974; Verbitskii and Vakhrushev, 1975; Darton, 1985) characterizes the medium in terms of an effective viscosity, largely a function of the voidage and less extensively of the particle size. The concept, however, is often invalidated: when examining Darton and Harrison's (1974) data, for instance, Fan and Tsuchiya (1990) noted that for 0.55-mm silica sand particles at high bed voidages (> 0.53), small bubbles ($d_e < 10$ mm) rose faster than they would have through a "fictitious" homogeneous medium; for the same particles at low voidages (< 0.50), the small bubbles rose much slower than they would have through an equivalent Newtonian medium. Darton (1985) ascribed this latter effect to non-Newtonian (pseudoplastic) behavior of the fluidized beds near the point of incipient fluidization. At expansions only slightly above the incipient fluidization, particle properties such as size, size distribution, density, and/or shape can be the predominating factors in determining the liquid-solid bed behavior.

Correspondence concerning this article should be addressed to K. Tsuchiya.

As for the particle-size effect, Tsuchiya et al. (1990) found that for a two-dimensional water-fluidized bed containing glass beads (diameter 0.163, 0.326, 0.460, 0.774 and 1.00 mm; density 2,500–2,780 kg/m^3) and acetate balls (1.50 mm; 1,250 kg/m^3), the bubble rise velocity was a function of the particle terminal velocity in addition to the solids holdup and bubble size, over the respective ranges of $U_t = 17.4$–169 mm/s, $\epsilon_s = 0.25$–0.51, and $d_e \approx 8$–30 mm. Covering similar particle properties (glass beads of 0.163–2.0 mm diameter) but a wider bubble-size range ($2.5 < d_e < 20$ mm) in a three-dimensional water-fluidized bed, Jang (1989) noted, at a high solids holdup ($\epsilon_s = 0.52$), a drastic reduction in the bubble rise velocity for small bubbles ($d_e < 5$ mm) due to the presence of particles, provided $d_p \geq 0.46$ mm, regardless of the particle size; for larger bubbles the rise velocity approached that in water as d_p decreased. At a low solids holdup ($\epsilon_s = 0.42$), the extent of the reduction either decreased with decreasing d_p for $d_e < 7$ mm or was less appreciable and only a week function of d_p for larger bubbles.

The effect of particle density was examined by Bly and Worden (1992), covering the density ranges of 1,015–1,460 kg/m^3 (gel beads of 2.6–3.2 mm diameter) and 2,500 kg/m^3 (glass beads of 3.0 mm diameter) and the bubble-size range $0.7 < d_e < 20$ mm. Bly and Worden accounted for the extent of reduction in the bubble rise velocity due to the presence of the solid phase by introducing a virial expansion in the solids holdup in their proposed correlation. The first- and second-order virial coefficients depended not only on the particle terminal velocity, which ranged from 18.6 to 334 mm/s and represented mainly the density effect, but strongly on the bubble size for $d_e < 6$ mm.

No systematic studies are available regarding the particle-shape effect on the bubble rise. Fan and Tsuchiya (1990) compared the data obtained by Jang (1989) for glass beads (spherical) and those by Darton and Harrison (1974) for silica sand (nonspherical) particles to find the appreciable differences between them, especially at small values of d_e (< 10 mm) as well as at high solids holdups ($\epsilon_s > 0.5$). They did not, however, provide any quantitative (or even physical) account of this shape effect that becomes very significant as the interparticle friction increases, thus warranting further research on this aspect.

The present study aims at providing both mechanistic insight into and quantitative data on the particle-shape effect at various bed voidages near incipient fluidization of spherical and nonspherical particles. Experiments were conducted in a two-dimensional column to directly observe the possible relationship between the rate and the tortuous path of bubble rise. The tortuosity of the bubble rise path, which can measure strong bubble–particle interactions prevailing near the incipient fluidization, is defined and incorporated in accounting for the marked reduction in the bubble rise velocity observed in both the present experiments and the literature (three-dimensional) results.

Experimental Studies

Figure 1 shows a schematic diagram of the experimental setup used in this study. The two-dimensional column is made of transparent polyvinyl chloride (PVC) and has the main section of 1.2-m effective height, 0.218-m width, and 14-mm

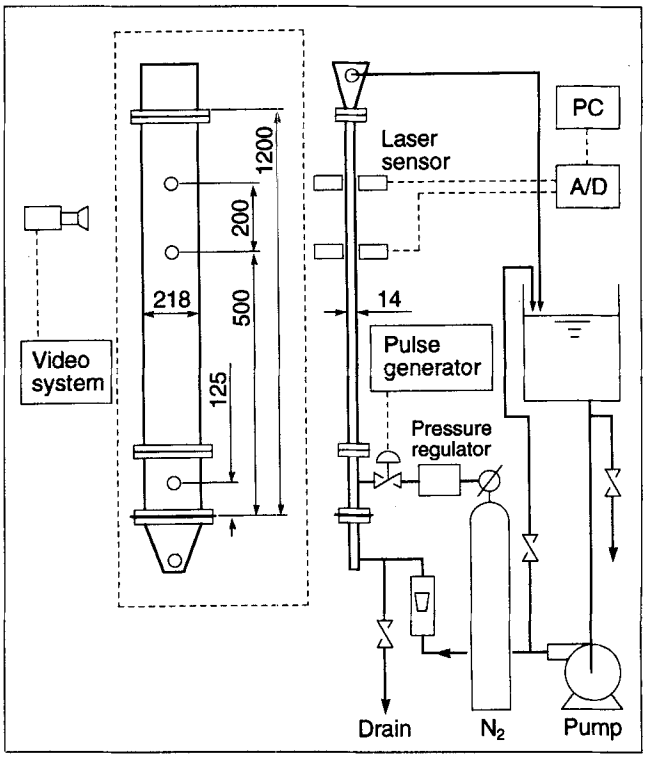

Figure 1. Experimental apparatus.

gap thickness. Below this section is the liquid distributing section, which consists of a packed bed of glass beads in double layers (6- and 3-mm beads in the lower and upper layers, respectively) confined in the tapered portion and a 5-mm-thick PMMA porous plate of 30-μm pore size and 35% porosity (Spacy Chemical, Inc., Tokyo). Gas injection is achieved through a 4.0-mm-ID stainless steel nozzle, with a tapered outlet, flush-mounted on the rear wall at a distance of 125 mm above the liquid distributor plate. A single bubble with no satellites can be readily generated; the bubble size is controlled roughly by altering the opening time of a solenoid valve, which is regulated by an electric pulse-signal generator, and precisely by regulating the gas delivery pressure with a digital pressure gauge of ± 10 Pa precision (Tokyo Kokukeiki DG-610, Japan). The top of the column is the liquid-solid disengagement section with another tapering so as to effectively settle the particles carried by the bubble.

The bubble rise characteristics, including the rise velocity, the major axis (breadth) and minor axis (height), and the rise path (trajectory of the bubble center), are measured by analyzing frame-by-frame the recorded video images obtained by a video camera (Sony CCD-TR55) fixed mostly at a location between 0.5 and 0.7 m above the liquid distributor; all the images are obtained over an exposure time of 1/1,000 s at 30 frames/s. A separate measurement of the bubble rise velocity is carried out, for limited runs, using a pair of laser sensors—one positioned 0.5 m above the liquid distributor and the other 200 mm further above. The sensor (Omron Z4LA-1030) consists of a light emitter [laser diode (LD); 780 nm, 3 mW], which can generate a parallel laser sheet that is 10 mm wide and 1 mm thick over the detectable distance of

Table 1. Physical Properties and Holdup of Solid Particles

Particle	U_t (10^{-2} m/s)	ϵ_s	ϵ_s/ϵ_{s0}
Glass beads (GB550)	0.493	0.564	0.934
$d_p = 0.55$ mm	0.616	0.550	0.911
$\rho_s = 2{,}490$ kg/m^3	0.684	0.523	0.866
$U_t = 82.5$ mm/s*	1.04	0.466	0.772
$U_{mf} = 2.65$ mm/s**	2.46	0.301	0.498
$\epsilon_{s0} = 0.604$			
Silica sand (SD550)	0.493	0.524	0.939
$d_p = 0.55$ mm	0.575	0.512	0.918
$\rho_s = 2{,}576$ kg/m^3	0.684	0.495	0.887
$U_t = 86.0$ mm/s*	0.821	0.472	0.864
$U_{mf} = 2.76$ mm/s**	0.958	0.455	0.815
$\epsilon_{s0} = 0.558$	1.09	0.435	0.780

* Estimated using correlation proposed by Clift et al. (1978) for spheres.
** Estimated using the Wen-Yu (1966) equation.

300 mm, and a light detector that has a 0.5-ms response time. The velocity values measured with this latter method have been confirmed to coincide with those determined based on the video frame analysis within $\pm 10\%$ error.

Nitrogen is used as the gas phase; the size of the single gas bubbles covered in this study ranges from 6 to 37 mm in equivalent diameter. The equivalent bubble diameter is defined as the diameter of a circle having the same area as the bubble area, which in reality is represented by the area projected onto the focused plane of visualization in the present apparatus, and estimated from the measured major and minor axes based on the assumption of an elliptic bubble shape, as recommended by Tsuchiya and Fan (1988). Comparing the measured and estimated bubble areas, Tsuchiya and Fan found that assuming a circular-cap shape overestimated its projected area even for a relatively large bubble due to the round edges of the actual bubble. Marked shape oscillations often observed for bubbles in the present size range are partially incorporated by considering the shapes averaged over several cycles.

Tap water is used as the liquid phase, the circulating flow of which (Figure 1) fluidizes the bed of one of two types of solid particles; Table 1 summarizes the physical properties and holdup of the particles as well as the superficial liquid velocity used for obtaining each specified solids holdup. All solids holdups are calculated from bed height. The solids holdup in the packed state ϵ_{s0}, in particular, is determined from the settled bed height after repeating the process of fluidizing, then carefully defluidizing the bed three times; for each batch of particles, loaded at a weight of $\sim$ 2.6 or 5.0 kg with a corresponding packing level $\sim$ 0.57 or 1.09 m, a deviation of at most ± 2 mm from the average of three replicates was found. All the experiments were conducted in the temperature range 20 ± 2°C.

Results and Discussion

Effect of solids holdup on rise velocity

Figure 2 shows the bubble rise velocity (U_b) obtained in the present fluidized bed containing various holdups of the spherical particles (GB550). The solids holdup covers as wide a range as $\epsilon_s = 0.30$–0.56. The plotted rise velocities have been made "relative" by subtracting the contribution of liquid upward flow, $U_t/(1-\epsilon_s)$, from the measured values (Darton

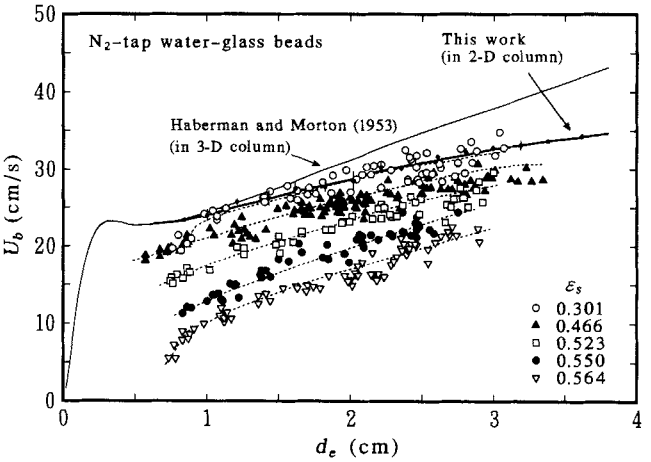

Figure 2. Bubble rise velocity in 2-D water–glass bead fluidized bed.
Solid lines for N_2(or air)–tap water system.

and Harrison, 1974). Note that each data point corresponds to one trial of bubble injection (although it is the average of three local measurements), plotting of which signifies the natural scattering associated with the inherent rise characteristics as well as the measurement errors. For comparison, Figure 2 includes two smoothed curves for bubbles in water —one obtained in the present 2-D system and the other representing the data of Haberman and Morton (1953), which are one of the most reliable sets of measurements (without any wall effect). The vertical/error bars crossing the former curve represent the standard deviation from average values taken over several trials with identical, or limited ranges of bubble sizes. As can be seen in the figure, for a given d_e the value of U_b in the water-solid medium approaches that in water as ϵ_s decreases. The effect of the solid particles becomes essentially null for $\epsilon_s < 0.3$, provided $d_e > 10$ mm.

Figure 3 shows U_b for the bed containing various holdups of the nonspherical particles (SD550). The ϵ_s range tested covers 0.43–0.52, narrower but with smaller increments than the case of GB550. The general trends exhibited in the figure

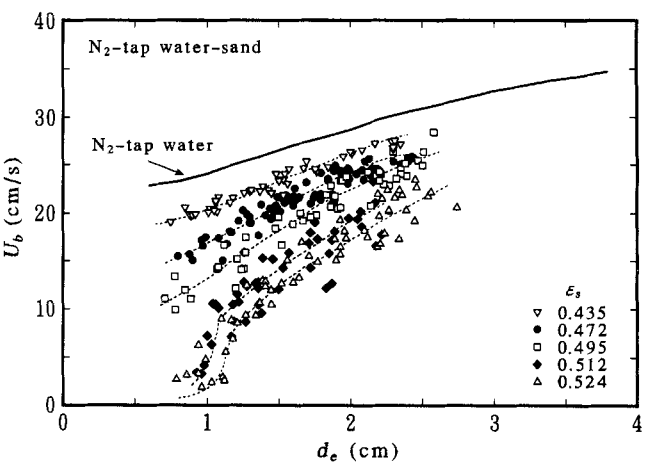

Figure 3. Bubble rise velocity in 2-D water–sand particle fluidized bed.

resemble those in Figure 2. An important feature to be noted in Figure 3 is that, for $\epsilon_s > 0.5$ (corresponding to 0.89 times ϵ_{s0}; see Table 1), the decrease in U_b with decreasing d_e, below critical values (≈ 12 mm), becomes drastic and extremely sensitive to the variation in d_e. A similar trend can be noted for GB550, although it is less obvious in Figure 2 [$\epsilon_s > 0.55$ (0.91 times ϵ_{s0}); $d_e < 8$ mm]. Since this feature is very crucial in estimating the rise velocity of small isolated bubbles in liquid-solid suspensions, a detailed discussion is presented in a separate section.

The preceding 2-D data inevitably involve wall effects, which would need to be corrected if they were compared with the literature (3-D) data. In the present study, however, no correction is made since the main objective is to elucidate the net shape effect for particles tested in the same apparatus under almost identical conditions (Table 1). It suffices to say that the extent of wall effect can be roughly estimated by comparing the two solid curves in Figure 2, even though the exact influence of the presence of particles cannot be evaluated. Furthermore, the fixed particle diameter of 0.55 mm, which is less than 1/25 of the column gap thickness, is believed to be sufficiently small to assure that this particle's contribution to the wall effect is minimal. This has been partially confirmed in this study.

Effect of particle shape on rise characteristics

Basis for Comparison. To elucidate possible differences in the bubble rise characteristics due exclusively to the particle shape between the GB550 and SD550, the solids concentration in addition to the particle size and density needs to be matched. In Figure 4 these two cases are compared when the solids holdup *relative to* that at the packed state/incipient fluidization, ϵ_s/ϵ_{s0}, is selected as the basis for comparison. No appreciable differences in U_b exist provided that the ϵ_s/ϵ_{s0} value is low (≈ 0.87) or, at higher ϵ_s/ϵ_{s0} (≈ 0.94), the bubble size is large ($d_e > 15$ mm). Note that, if the same *absolute* holdup were used instead, there would clearly be a difference since ϵ_{s0} differs in the two cases (Table 1). These trends are reasonable since:

1. The close-range interactions between particles (of irregular shapes in particular)—not only simple impacts but also harsh surface friction such as interlocking or scraping—should be controlled by the interparticle distance *relative to* that in the packed state.
2. At low solids concentrations (that is, large interparticle distances), these close-range interactions (thus the particle-shape effects) diminish.
3. The static pressure near the frontal surface of a fast-rising large bubble is modified (or more specifically, increased)—due to the presence of this "obstacle"—to a great extent. This pressure modification can result in an increase in the form drag exerted upward on the nearby particles, and thus tends to reduce the extent of surface-domain interactions between the bubble and the particles.

On the basis of these comparisons, the net effect of particle shape was examined in this study under the conditions of identical ranges of particle size, particle density, and the normalized solids holdup ϵ_s/ϵ_{s0}.

Difference in Bubble Rise Path. Based on the experimental results presented so far, two distinctive characteristics regarding the reduction in the bubble rise velocity in the presence of solid particles are recognizable: (1) "general" reduction whose extent is mainly a function of the solids holdup [besides the particle terminal velocity (Tsuchiya et al., 1990)] and independent of the particle shape; (2) "peculiar" reduction whose extent depends strongly on the particle shape. The first type of reduction in U_b is observed in a moderate range of ϵ_s ($0.3 < \epsilon_s < 0.9\epsilon_{s0}$) over almost the whole range of bubble sizes examined in this study. The second type, on the other hand, is extremely sensitive to the bubble size (thus to the bubble hydrodynamics) as well as the particle shape and solids holdup.

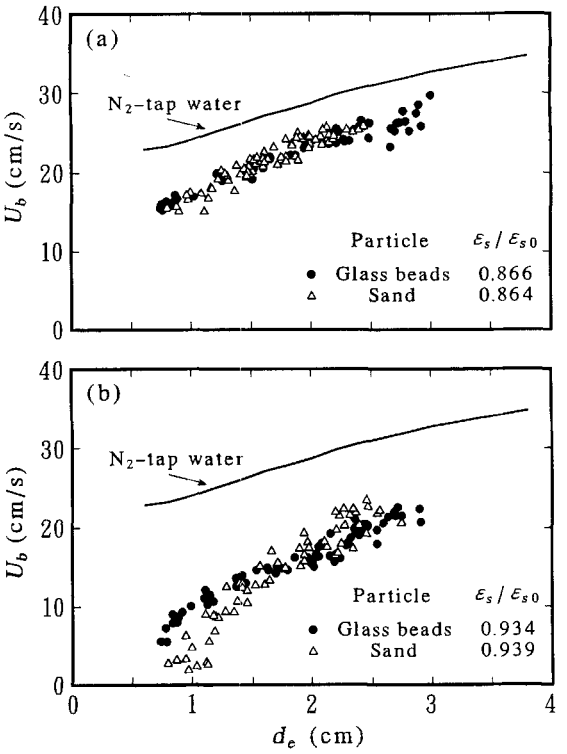

Figure 4. Particle-shape effect evaluated with normalized solids holdup as the basis for comparison at (a) intermediate and (b) high values of ϵ_s/ϵ_{s0}.

Important clues to the mechanisms for such particle effects can be partially identified by examining the path and rate of bubble rise simultaneously. Figures 5 and 6 depict typical traces of the bubble rise paths starting from arbitrary points [in the experiments, conveniently fixed mostly at heights between 0.50 and 0.55 m; in the figures, fixed at $(y, z) = (0, 0)$] for values of $\epsilon_s/\epsilon_{s0} = 0.865$ and 0.935, respectively. The former value is below the critical $\epsilon_s/\epsilon_{s0} \approx 0.9$ demarcating the two types of U_b reduction. Both figures are obtained for bubble sizes of (a) $d_e = 17$ mm (large bubble) and (b) $d_e = 10.5$ mm (small one) in the presence of no solids, the glass beads, and the sand particles. As seen in Figure 5 (and expected), no drastic differences in the bubble rise path are noticeable between the three cases except a typical, regular sinusoidal path (with a larger amplitude) observed for the smaller bubble in water (Figure 5b). The rate of bubble rise is comparable between the two cases with solids in contrast to the case

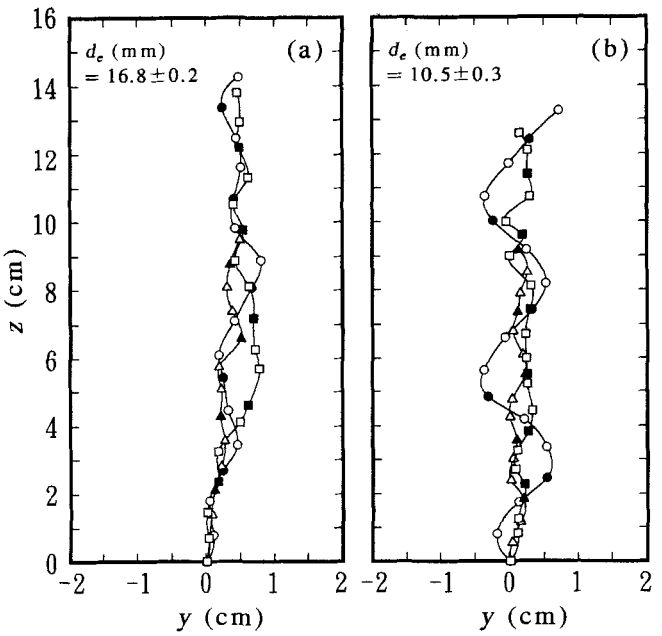

Figure 5. Typical traces of bubble rise paths at intermediate ϵ_s/ϵ_{s0} (=0.865±0.01) for (a) large and (b) small bubbles.

Key: circles for no solids; triangles for GB550; squares for SD550; open symbols for every 1/30 s; filled symbols for every 1/10 s.

without them (compare the vertical locations of solid symbols, which mark 0.1-s intervals, that is, every 3 frames of the video recordings).

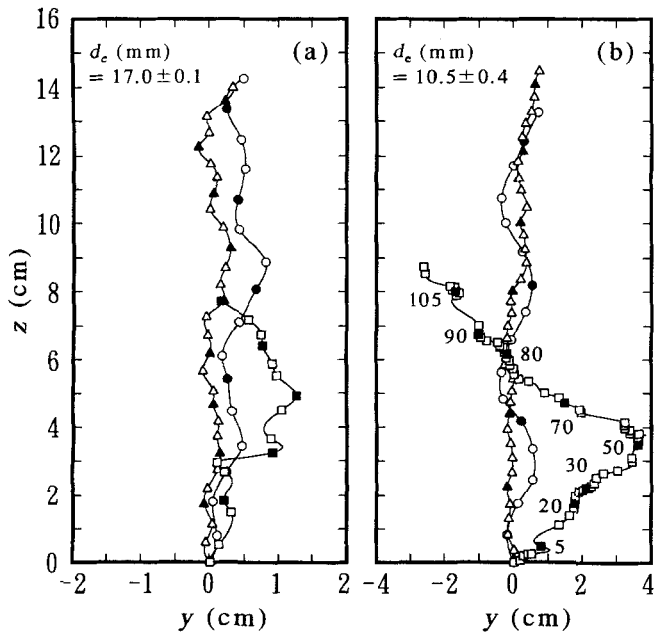

Figure 6. Typical traces of bubble rise paths at high ϵ_s/ϵ_{s0} (=0.935±0.04) for (a) large and (b) small bubbles.

Key: circles for no solids; triangles for GB550; squares for SD550; open symbols for every 1/30 s; filled symbols for every 1/6 s.

For the latter value of ϵ_s/ϵ_{s0}, that is, above the critical value (Figure 6), a peculiarity in the rise path can be specifically noticed for SD550; while the bubble rising in either water or the water-GB550 fluidized bed has a similar rise path, dominated by the vertical rise, the one in the water-SD550 medium "detours" appreciably. The net rise velocity differs appreciably as well. The difference between water and the water-GB550 medium amounts to as much as twofold in U_b (compare the vertical locations of solid circles and triangles, which mark 0.167-s intervals, that is, every 5 frames of the video recordings, in Figure 6b). In the case of water-SD550 medium, the reduction in U_b is so large that it takes the bubble about 10 times as long to travel upward as it does in water (refer to the numbers beside the solid squares, which indicate the frame numbers).

Tortuosity of bubble rise path

The difference in the bubble rise path, analyzed so far only qualitatively, is now quantified in terms of "tortuosity." The tortuosity of the rise path is defined in this study as the ratio of the total distance to the net vertical distance traveled by a bubble. The actual calculation is performed by first obtaining the pair of distances in each (minimum) interval of time, 1/30 s in this study, then summing the consecutive distances separately, and taking the ratio of the two summations to yield:

$$\tau_N = \sum_{i=1}^{N} \sqrt{(y_i - y_{i-1})^2 + (z_i - z_{i-1})^2} \Big/ \sum_{i=1}^{N} (z_i - z_{i-1}) \quad (1)$$

where N is the total number of intervals used for the calculation, which is repeated until the value of tortuosity converges to an asymptotic value τ independent of the value of N.

For bubbles rising in water, the convergence can be obtained for N within 2–12 intervals, depending on the bubble size. Bubbles of $d_e \approx 12$–15 mm, for example, need a longer time to attain the asymptotic values; τ_N varies with N in a sinusoidal (with decaying amplitude) manner, which corresponds to the zigzag rise path, and gradually converges after several cycles of oscillation. In the water-GB550 medium, the tortuosity exhibits a similar trend with respect to N, but takes persistently smaller values. In the water-SD550 medium, it takes a much longer time for the tortuosity calculated from Eq. 1 to converge. This trend reflects the very peculiarity/intricacy of the rise path depicted in Figure 6b.

Bubble-Size Effect. The asymptotic values of τ are plotted against d_e in Figures 7 and 8. The data for water (Figure 7a) exhibit distinctive features in their trend, especially in the d_e range from 13 to 15 mm; the comparatively large scatter in the τ value reflects the observed difference in the extent of oscillations in the rise path, which interrelate closely to the rather abrupt, large shape oscillations occasionally observed in this particular range. Below this range, τ increases slightly with d_e; as d_e reaches 15 mm (the corresponding bubble Reynolds number $Re = d_e U_b/\nu_l \approx 4{,}000$), τ suddenly drops to values barely exceeding unity. As d_e exceeds this critical size, the tortuosity remains nearly unity, corresponding to the rectilinear rise of large circular-cap bubbles of high stability.

In the presence of the spherical GB550 (Figure 7b to 7d), the tortuosity appears to be a weak function of the bubble size for $7 < d_e < 25$ mm; in addition, it takes consistently lower

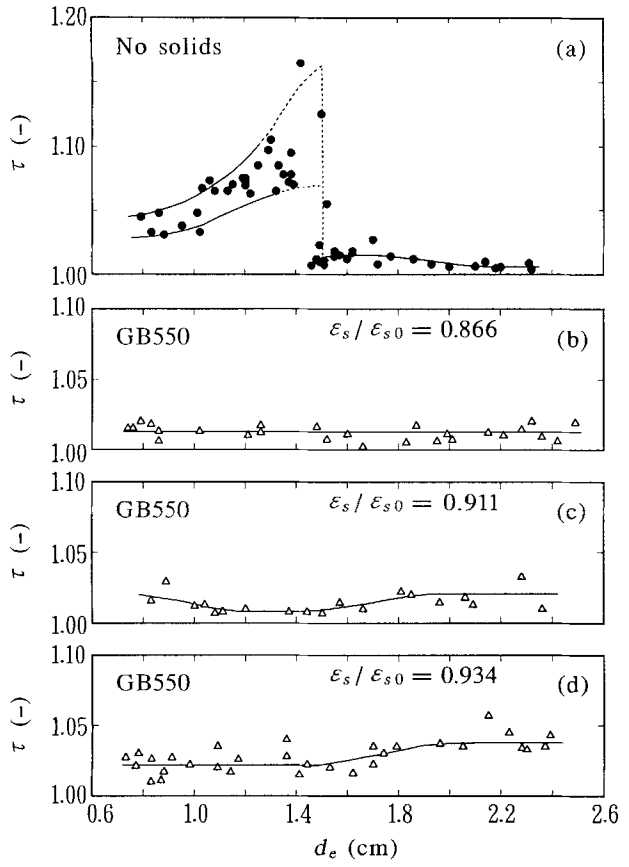

Figure 7. Tortuosity as a function of bubble size for bubbles in (a) water and (b)–(d) water-glass bead fluidized bed at various solids holdups.

The broken part of lines signifies uncertainty associated with scattered data points.

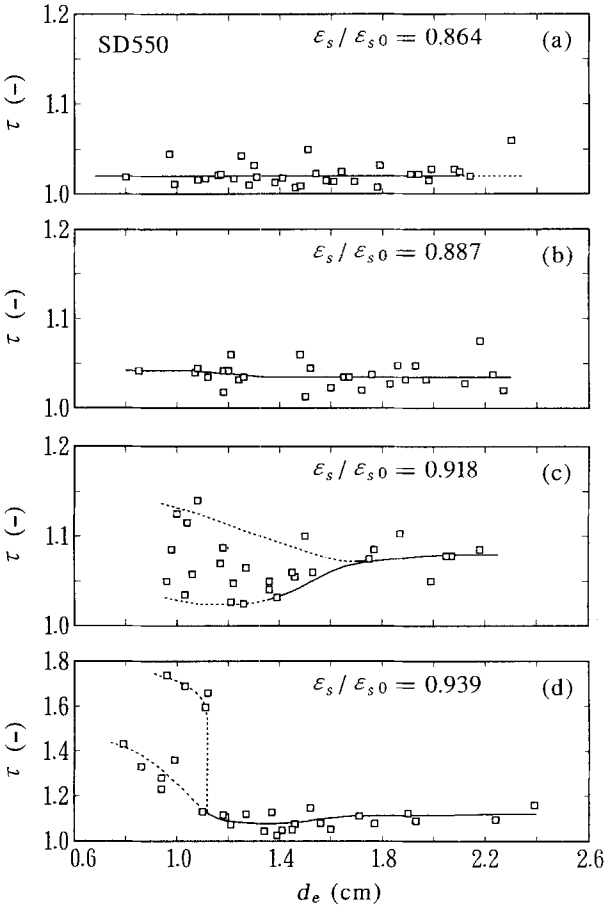

Figure 8. Tortuosity as a function of bubble size for bubbles in water–sand particle fluidized bed at various solids holdups.

The broken part of lines signifies uncertainty associated with scattered data points.

values than in water when the bubble oscillations are supposed to be extensive—as if the bubbles rose in a homogeneous medium of viscosity higher than that of water alone. The average τ value over the given d_e range increases slightly with ϵ_s/ϵ_{s0}. Another point to be noted is that for large bubbles ($d_e > 18$ mm), while τ settles down to unity in the absence of solids (Figure 7a), their presence does not lead to the same trend or even results in apparently the opposite trend at high ϵ_s/ϵ_{s0} (Figure 7d). This apparent increase in the tortuosity for large circular-cap bubbles rising under inertia/gravity domain, however, is found not to affect the rise velocity.

In a similar series of plots (Figure 8a to 8d) for the nonspherical SD550, on the other hand, a drastic difference in the tortuosity behavior is apparent: while the bubble size-independent behavior prevails as long as ϵ_s/ϵ_{s0} is below the critical value of 0.9, τ abruptly increases from ~ 1.1 to as large as 1.7 (or apparent coexistence of roughly two separate values of $\tau \sim 1.6$ and 1.3) as d_e is reduced below 12 mm by just a couple of millimeters at the highest solids holdup (Figure 8d). This anomaly, with its precursory behavior (a relatively large scatter in τ) already apparent at ϵ_s/ϵ_{s0} slightly above the critical value (Figure 8c), vastly differs from the behavior in water or the water-GB550 medium [at least in the bubble-size range (> 7 mm) investigated in this study]. Under such conditions, the overwhelmingly tortuous rise path experienced by small bubbles (with low inertia) can be a major factor responsible for the drastic reduction in U_b—effected in this study for $d_e < 12$ mm by the difference in the particle shape between GB550 and SD550 (see Figure 4b).

The nonuniqueness of the tortuosity in concentrated suspensions (for bubbles of $d_e < 12$ mm in the SD550 medium or possibly for $d_e < 8$ mm in the GB550) is suspected to result from the peculiar "detouring" in the rise path combined with the occasionally occurring "hesitation" in the net vertical movement. Figure 9 shows the detailed rise paths of six bubbles of slightly different sizes in a small interval of d_e ranging from 8.6 to 11.2 mm. The first group of bubbles (circles) exhibit very tortuous routes—characteristic of bubbles' finding the least-resistant pathway from moment to moment upon constantly changing voidage/viscosity of the surrounding medium (Darton and Harrison, 1974). The second group (triangles) follow comparatively less tortuous paths. The last one (a square), which rises exceptionally fast at $U_b \approx 9$ cm/s, exhibits an almost rectilinear path. All these types of rise paths, however, involve recurring hesitation; the degree of the hesi-

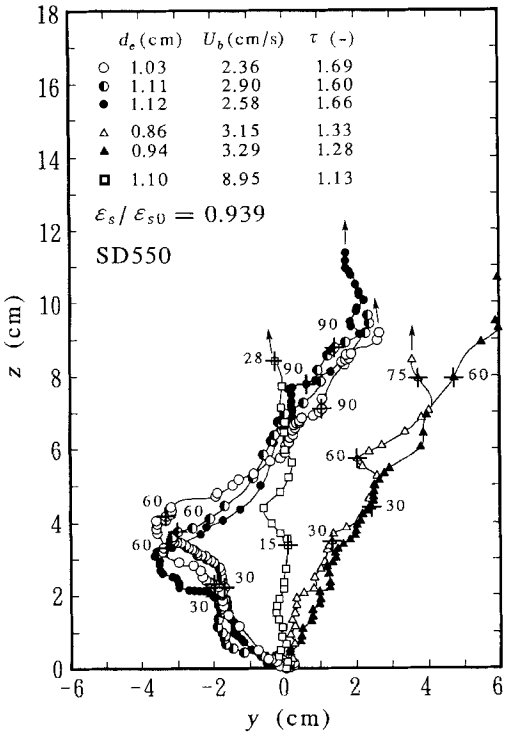

Figure 9. Traces of rise paths of bubbles of slightly different sizes in water–sand particle fluidized bed at high solids holdup.

tation, which is a measure of the resistive stresses and another major factor responsible for the drastic reduction in U_b, does vary from bubble to bubble; the smaller the bubble, in general, the higher the degree of the hesitation [compare the (frame) numbers beside the cross symbols].

Concluding Remarks

The particle-shape effect on the bubble rise velocity is significant for small bubbles rising in concentrated liquid-solid suspensions where the close-range (surface-to-surface) interactions between the particles play a crucial role. In this study which covers the bubble-size range of 6–37 mm and solids holdups as high as 0.94 times that in the packed state, such interactions are found to be appreciable for the relative solids holdups exceeding 0.9. The maximum bubble size below which the bubble rise velocity is reduced to an unusual extent is ~ 12 and 8 mm for the irregular sand and spherical glass particles, respectively. This anomalous reduction in the rise velocity stems partly from the tortuousness in the rise path and partly from the "hesitation" in the net vertical movement. The former, in particular, is quantified in terms of the tortuosity estimated directly from the visual information on the two-dimensional rise path. The results are found to support, at least partially, the peculiar reduction in the rise velocity of small bubbles observed, especially for the sand particles.

Notation

d_p = particle diameter, m
U_l = superficial liquid velocity, $m \cdot s^{-1}$
U_{mf} = superficial liquid velocity required to achieve minimum fluidization, $m \cdot s^{-1}$
y = horizontal righthand distance from the vertical axis passing through bubble center at the moment of starting bubble-path tracing, m
n = vertical upward distance from the starting point of bubble-path tracing, m

Greek letters

ν_l = liquid kinematic viscosity, $m^2 \cdot s^{-1}$
ρ_s = solid density, $kg \cdot m^{-3}$
τ = tortuosity of bubble rise path (asymptotic value)

Literature Cited

Bly, M. J., and R. M. Worden, "The Effects of Solids Density and Void Fraction on the Bubble Rise Velocity in a Liquid-Solid Fluidized Bed," *Chem. Eng. Sci.*, **47**, 3281 (1992).

Clift, R., J. R. Grace, and M. E. Weber, *Bubbles, Drops, and Particles*, Academic Press, New York (1978).

Darton, R. C., "The Physical Behaviour of Three-Phase Fluidized Beds," *Fluidization*, 2nd ed., Chap. 15, J. F. Davidson, R. Clift, and D. Harrison, eds., Academic Press, London, p. 495 (1985).

Darton, R. C., and D. Harrison, "The Rise of Single Gas Bubbles in Liquid Fluidized Beds," *Trans. Inst. Chem. Eng.*, **52**, 301 (1974).

El-Temtamy, S. A., and N. Epstein, "Rise Velocities of Large Single Two-Dimensional and Three-Dimensional Gas Bubbles in Liquids and in Liquid Fluidized Beds," *Chem. Eng. J.*, **19**, 153 (1980).

Fan, L.-S., and K. Tsuchiya, *Bubble Wake Dynamics in Liquids and Liquid-Solid Suspensions*, Butterworth-Heinemann, Stoneham, MA (1990).

Haberman, W. L., and R. K. Morton, "An Experimental Investigation of the Drag and Shape of Air Bubbles Rising in Various Liquids," *David W. Taylor Model Basin* Report 802, Navy Dept., Washington, DC (1953).

Henriksen, H. K., and K. Ostergaard, "Characteristics of Large Two-Dimensional Air Bubbles in Liquids and in Three-Phase Fluidized Beds," *Chem. Eng. J.*, **7**, 141 (1974).

Higbie, R., "The Rate of Absorption of a Pure Gas into a Still Liquid during Short Periods of Exposure," *Trans. AIChE*, **35**, 365 (1935).

Jang, C.-S., "Hydrodynamics of Liquid-Solid Fluidization," MS Thesis, Ohio State Univ., Columbus (1989).

Jean, R.-H., and L.-S. Fan, "Rise Velocity and Gas-Liquid Mass Transfer of a Single Large Bubble in Liquids and Liquid-Solid Fluidized Beds," *Chem. Eng. Sci.*, **45**, 1057 (1990).

Massimilla, L., A. Solimando, and E. Squillace, "Gas Dispersion in Solid-Liquid Fluidized Beds," *Brit. Chem. Eng.*, **6**, 232 (1961).

Tsuchiya, K., and L.-S. Fan, "Near-Wake Structure of a Single Gas Bubble in a Two-Dimensional Liquid-Solid Fluidized Bed: Vortex Shedding and Wake Size Variation," *Chem. Eng. Sci.*, **43**, 1167 (1988).

Tsuchiya, K., G.-H. Song, and L.-S. Fan, "Effects of Particle Properties on Bubble Rise and Wake in a Two-Dimensional Liquid-Solid Fluidized Bed," *Chem. Eng. Sci.*, **45**, 1429 (1990).

Verbitskii, B. G., and I. A. Vakhrushev, "Ascent Velocity of Single Gas Bubbles in a Liquid-Fluidized Bed," *Int. Chem. Eng.*, **15**, 277 (1975).

Wen, C. Y., and Y. H. Yu, "Mechanics of Fluidization," *Chem. Eng. Progr. Symp. Ser.*, **62**, 100 (1966).

Manuscript received Feb. 22, 1994, and revision received June 6, 1994.